REAL-TIME PHYSICAL MODEL OF A WURLITZER AND RHODES ELECTRIC PIANO

Florian Pfeifle

Systematic Musicology,
University of Hamburg
Hamburg, DE
Florian.Pfeifle@uni-hamburg.de

ABSTRACT

Two well known examples of electro-acoustical keyboards played since the 60s to the present day are the Wurlitzer electric piano and the Rhodes piano. They are used in such diverse musical genres as Jazz, Funk, Fusion or Pop as well as in modern Electronic and Dance music. Due to the popularity of their unique sound and timbre, there exist various hardware and software emulations which are either based on a physical model or consist of a sample based method for sound generation. In this paper, a real-time physical model implementation of both instruments using field programmable gate array (FPGA) hardware is presented. The work presented herein is an extension of simplified models published before. Both implementations consist of a physical model of the main acoustic sound production parts as well as a model for the electromagnetic pickup system. Both models are compared to a series of measurements and show good accordance with their analog counterparts.

1. INTRODUCTION

Electromechanical and analog electric systems used for musical sound generation were building blocks of early types of electronic music instruments from the late 19th century well into the second half of the 20th century. Largely driven by the advances in science and engineering as well as the rising capabilities of music recording, transmission and reproduction systems, these instruments were crucial for the evolution of various modern music styles and were formative ingredients for multiple music genres. Two prominent electromechanical keyboard instruments from the 1960s and 1970s that are still being used in modern music productions are the Fender Rhodes and the Wurlitzer electronic piano. Their unique sound can be heard in many well known songs from genres such as Jazz, Funk, Pop, Rock and modern electronic music as well. Due to the fact that central parts of modern music production, recording and transmission gradually shifted from analog to fully digital processing chains from the late 20th century on, these two instruments are popular options for digital emulations in synthesizers, digital keyboards and hardware/software samplers of differing product generations and vendors. Notwithstanding the availability of a multitude of different emulations on various hardware and software platforms , there is an ongoing effort to optimize models of musical instrument towards physical plausibility and realistic sounding simulations of analog instruments in general as well as the Rhodes and Wurlitzer in special.

In this paper, a methodology and implementation of a Fender Rhodes and Wurlitzer e-piano's sound production system implemented on field programmable gate array (FPGA) hardware is presented. The implementation is based on a physical model published in [18], [17], [19] and uses a similar hardware implementation methodology as is published in [21]. This work aims at extending the existing physical models of mentioned publications in two regards by (**1**) implementing them on a FPGA for real-time synthesis and (**2**) making the physical model more accurate when compared to physical measurements as is discussed in more detail in section 4 and 5.

2. RELATED WORK

Scientific research regarding acoustic and electro-mechanic properties of both instruments is comparably sparse. Freely available user manuals as well as patents surrounding the tone production of the instruments give an overview of basic physical properties of both instrument [5]; [7]; [8]; [13]; [4]. The operation manual of the Rhodes contains several important aspects of its construction and explains influences of mechanical properties and the resulting effects on the sound of the instrument, see [11]. The Wurlitzer's manual gives a comprehensive overview and reference on the construction of the instruments and the resulting sound, see [25]. As is shown in [18], some of these publications fail to explain the influence of certain physical effects in the formation of the sound.

Regarding a scientific classification of the acoustic and electronic properties of the Rhodes and Wurlitzer piano there are several works that can be highlighted here. A thesis , available in German only, highlights acoustic features of the Rhodes by focussing on the vibration of the tine and the resulting sound [10]. Some non-linear properties and effects of the rhodes' tone production is published in [19] and [17]. A physical model of Rhodes' tone production using a Port-Hamiltonian approach is presented in [27]. Acoustic properties taken from high-speed camera measurements and finite difference models of both instruments are published in [18].

3. PHYSICAL PROPERTIES

This section gives an overview on on physical properties of the main sound producing parts of both instruments. The measurements presented here are based on work published in [18] as well as more recent measurements performed on the same instruments.

3.1. Tone production mechanism in the Fender Rhodes

The Fender Rhodes measured in this work is used as a foundation for the model presented in section 5. It is comparable to most Rhodes' electronic pianos from the late 60s to the early 80s.

The mechanical part consists of a rod made of spring steel shrunk into an aluminium block on one side, making the resulting system comparable to a cantilever beam. The length and circumference of the rod as well as the position of a small tuning

spring, adding mass, determines its fundamental frequency. The rod, which in the case of the Rhodes piano is called a tine, is excited by hammer having a neoprene tip. The key action mechanism is a simplified single action as described in [6], it can be compared to a *Viennese* or *German* piano action because the hammer is in direct contact with the key. Depending on the year of construction the key and hammer mechanisms are crafted from wood or, as is generally used in newer models, of synthetic materials. Every tine is damped by an individual felt damper that is in contact with the tines from below. The fixation of the tine, the aluminium block, is tightly connected to a, sometimes $\frac{\pi}{2}$ twisted, brass bar which acts as the second prong of the patented Rhodes' "tuning fork" system.

The harmonic oscillations of the mechanic part of the Rhodes' tone production is converted to an alternating voltage by an electromagnetic pickup that consists of a wound permanent magnet. This setup is comparable to a pickup of a guitar in its overall structure but differs in terms of the geometry of the magnets tip as is depicted in Figure 1.

The geometry of the pickup's iron tip shapes the specific distribution of the magnetic field in which the tine vibrates. The motion of the ferromagnetic tine changes the flux of the magnetic field which in turn produces a change in the electromotive force of the pickup. This results in an alternating voltage which then can be amplified by an external amplifier. The copper wire winding of each pick up is divided into two sections, connected in opposite phase for hum cancelling.

The timbre of a Rhodes note can be altered by changing the position of the tine in respect to the magnet as schematically depicted in Figure 7**a** and Figure 7**b**.

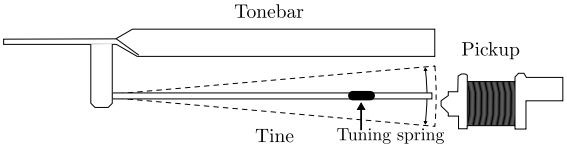

Figure 1: The Rhodes Tuning Fork assembly with electromagnetic pickup.

3.2. Tone production mechanism in the Wurlitzer

Compared to the Rhodes piano, the tone production mechanism in the Wurlitzer piano is based on a different physical principle . In contrast to the Rhodes' picks-up which reacts to changes in the magnetic field (H-field), the Wurlitzer's pickup system is designed to detect changes in the E-field distribution over the sound generators geometry. In special, it is designed as a time-varying capacitor which consists of a loaded static plate and a moving plate, called a reed [25], having zero potential (connected to ground). Mechanically the reed is fixed at one side and free on all others. According to the manual, the high potential has a voltage 170V which has been found to be considerably lower (130V) in the measured instrument used in this work. Effectively, the time varying capacitance induces a time-varying current which in turn induces a time-varying voltage which is being amplified by the subsequent amplification circuit.

There are two factors determining the fundamental frequency f_0 of every reed, the physical dimensions of the reed itself and the amount of solder on the tip of the reed. By removing or adding lead to the tip of the reed its f_0 is increased or lowered respectively.

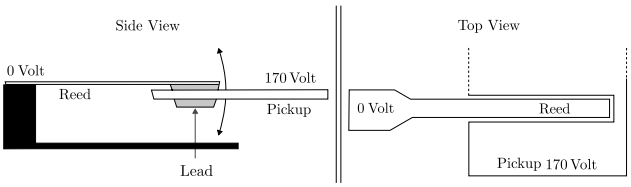

Figure 2: Structural depiction of the Wurlitzers pickup system. A side view on the left, top view on the rigth. Both showing the high potential plate and the low potential reed.

As is depicted in Figure 2, the charged plate has cutouts at the position of the reed for each note of the instrument. The reeds are designed to vibrate freely between the symmetric cutouts, providing a surface area large enough to produce a measurable change in capacity. The air gaps between plate and reed act as dielectric material. Analogous to the case of a plate capacitor or the diaphragm of a condenser microphone, the capacity varies inversely proportional to the distance between the two electrodes, in this case: reed and fixed plate.

The key action mechanism of the Wurlitzer piano consists of a miniaturized London style piano action that can be regulated like a grand piano action. Every reed of the Wurlitzer electric piano is excited by an individual ply maple hammer that has a felt tip [25]. Comparable to the playing dynamics of the Rhodes piano, depressing the keys with higher velocity results in a richer harmonic sound of the Wurlitzer than playing softly.

4. MEASUREMENTS

4.1. Measurement tools

All measurements of visibly moving parts of both instrument's primary sound production parts are performed using a *Vision Research* V711 high-speed camera. The recorded motion is tracked with sub-pixel accuracy using *Innovision System*'s *MaxTraq2D* software. The traced trajectories are exported as time series which are post-processed and evaluated using the high-level language *julia*. Electronic properties are measured using a measurement amplifier and converter *LTT24* by *Tasler*. Analog sound outputs of both instruments are recorded using *Logic Pro X* software and a *Focusrite* interface running at 44,1kHz and 24 bit.

4.2. Rhodes measurements

As depicted in Figure 3, the tip of the tine vibrates in an approximately sinusoidal motion, the direct-out signal measured behind the pick-up has a more complex waveform, showing the influence of the magnetic field of the pick-up.

As an extension to the measurements in one plane, the same rhodes tine is measured with the camera in two horizontal dimensions. Figure 4 shows non-planar motion in the transversal direction. The tine's vibration in the vertical plane u_{ver}, which is the direction of the hammer impact, is larger when compared to that in the horizontal plane u_{hor}. The horizontal motion is excited either through coupling effects on the tine or due to imperfections in the hammer tip.

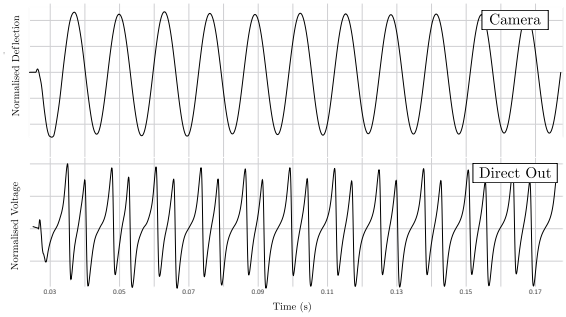

Figure 3: Measurement of one Rhodes tine. The upper row shows the deflection of the tine the lower the measured direct-out signal behind the pick-up.

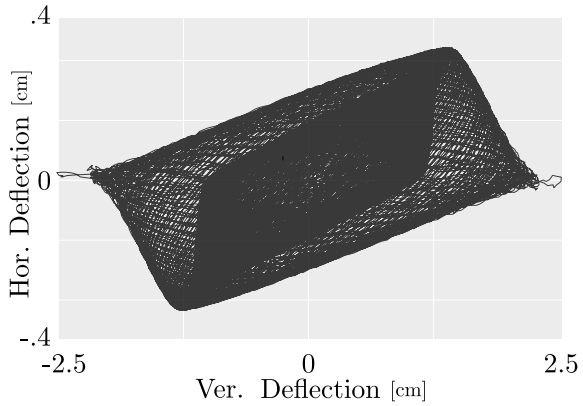

Figure 4: Phase plot of the two polarisations of the tine deflection of one tine.

4.3. Wurlitzer measurements

Figure 5 shows the first 12 milliseconds of the Wurlitzer's reed motion and the measured sound at the output.

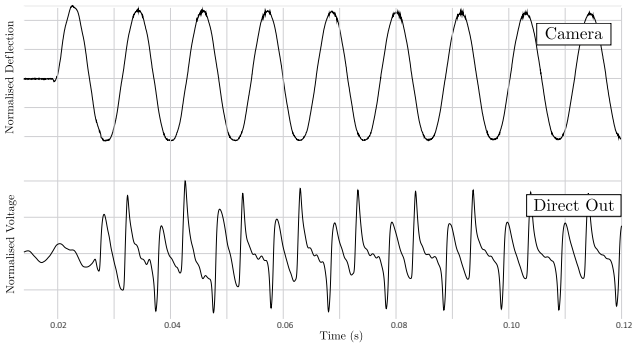

Figure 5: The upper graph shows the tracked camera signal having approximately sinusoidal motion. The lower graph shows the voltage measured behind the pick-up system before the amplification circuitry.

5. PHYSICAL MODEL

5.1. Overview

The physical models presented in this section are based on the measured properties presented in section 4, qualitative observations of the FEM models published in [18] and some assumptions regarding material properties of the Wurltizer's reed and the hammer tip of both instruments. The model of the Rhodes e-piano includes a formulation for the hammer impact, a model of a beam vibrating in two polarisations subject to large effects and a preprocessed approximation of the magnetic field distibution over the tip of the pick-up's magnet core. The model of the Wurlitzer EP200 shares conceptual similarities with the Rhodes model but is adapted to the different geometry of the sound production. The tine of the Wurlitzer is modeled as a non-uniform cantilever beam with large-deflection effects and a spatial transfer function describing the change in capacitance resulting from the motion of the tine.

5.2. Hammer model

A hammer impact including viscoelastic material properties of the hammer tip can be simulated by using a hysteretic hammer model as presented in [22] and [14]. This impact model is able to simulate hammer impacts of different materials showing viscoelastic behaviour. Based on the formulation in [14], a distributed force exerted by a hammer impact follows the relationship

$$F([\mathbf{x}],t) = \begin{cases} k \cdot \mathbf{x}(t)^{\alpha} + \lambda \cdot \mathbf{x}(t)^{\alpha} \cdot x_t(t) & \text{if } \sum_{xL} \mathbf{x} > 0 \\ 0 & \text{for } \sum_{xL} \mathbf{x} \leq 0 \end{cases} \quad (1)$$

with $\sum_{xL}$ indicating a weighted sum over the contact area. This model is based on a model for hammer impacts developed by Hunt & Crossly [33], that has been shown to yield good results for models of hammer impacts with moderate impact velocities and plain geometries [14]; [29]. Here, α is the nonlinearity exponent depending on the geometry of the contact area and λ is a material dependent damping term that dissipates energy in dependence to the velocity of the changing hammer-tip compression written as x_t.

5.3. Rhodes tine model

In an earlier work ([18]), the tine of the Rhodes was modeled as simple harmonic oscillator approximating it's fundamental motion. Here, the tine is modeled as a cantilever beam with non-planar motion, large-deflection effects, and inclusion of the tuning spring as an additional mass.

Large deflection effects are included by taking shearing effects in the beam into account. Trail & Nash [26] showed that the shear beam is a better approximation for the vibrations of the fundamental frequency then the more popular Euler-Bernoulli beam and less computationally complex as the similar accurate Timoshenko beam model. Coupling between two polarisations for large deflections of the beam can be included as proposed in [**?**]. Compared to its diameter, the deflection of the Rhodes' tine is large. Thus it is feasible to include high deflection effects into the formulation of the model. As shown in [28] the inclusion of shear effects to the Euler-Bernoulli beam raises the accuracy of the fundamental frequency as well as the accuracy of higher partials. Following the consideration in [28], the differential equation for a round beam

exhibiting large and non-planar deflections, having non homogeneous mass, and not considering the angle of rotation can be written as

$$\begin{aligned} \rho \mathbf{u}_{tt} \quad &+ \quad [\mathrm{EI}\mathbf{u}_{xx}]_{xx} - \mathrm{EA}\frac{1}{2}\mathbf{u}_{xx} \cdot K(\mathbf{u}) \\ &- \quad \kappa \mathbf{u}_{2x2t} - F(\mathbf{u}^V[x], t) = 0 \end{aligned} \tag{2}$$

Here, $\mathbf{u}$ is the deflection in two transverse polarisations (H, V), E is the Young's modulus I is the radius of gyration and A is the cross-sectional area. $F(\mathbf{u}^V[x], t)$ is the forcing function of the hammer model, impacting the bar in the vertical direction indicated by u^V. $K(u, w)$ is a nonlinear Kirchhoff-like term given as

$$K(\mathbf{u}) = \int_0^l (\mathbf{u}_x^H)^2 + (\mathbf{u}_x^V)^2 dx \tag{3}$$

5.4. Rhodes pickup model

As depicted in Figure 1 the tip of the tine vibrates in close proximity to the electromagnetic pickup and the FEM simulations given in Figure 8 of [18] highlight that only a small part of the tip is influenced by the magnetic field. For a derivation of the magnetic field distribution in two dimensions, the tip is approximated as a finite point oscillating over an idealised geometry of the magnetic pick-up tip.

The electromagnetic effects of the Rhodes' pickup system can be reduced from Maxwell's equations for transient electromagnetic effects to a more tractable formulation know as Faraday's law of induction. As shown above, the pickup consists of a magnetized steel tip and a coil wrapped permanent magnet; leaving reciprocal magnetic effects of the induced current in the coil out of our consideration, the voltage induced over the pickup is equivalent to the change of the magnetic flux in the field produced by the magnet

$$\epsilon = -\frac{\partial \Psi_{\mathbf{B}}}{\partial t} \tag{4}$$

with ϵ the electromotive force and Ψ_B the magnetic flux due to the change in the magnetic field given by

$$\Psi_{\mathbf{B}} = \int \vec{B} \cdot d\vec{S} \tag{5}$$

with B the magnetic field strength integrated over surface S. Using these equalities, the induced voltage directly depends on the change of magnetic field strength which depends solely on the position of the tine disturbing the field as shown in Figure 7.

The following derivation of the magnetic field distribution uses the unphysical assumption that there exist magnetic monopoles which produce a distributed magnetic field.[1] As is shown in [16] this approach yields good approximations of notional magnetic induction fields produced by guitar pickups (see also [15]). Consisting of a plainer geometry, the tip of a guitar pickup bar magnet can be simplified to a circular, magnetically charged disc with a certain cross-section, which reduces the problem to a position-dependent integration of the field over the pickup. Due to the specific pickup geometry of the Rhodes, a different approach is taken here to calculate the induction field strength above the tip of the magnet. As depicted in Figure 6 our derivation makes use of several simplifying assumptions facilitating the computation of the magnetic field distribution over the magnet's tip that are

1. The tine vibrates in an sinusoidal motion in both planes in in front of the pickup.
2. The tip of the tine vibrates on the trajectory of an ideal circle with the center at its fixation point.

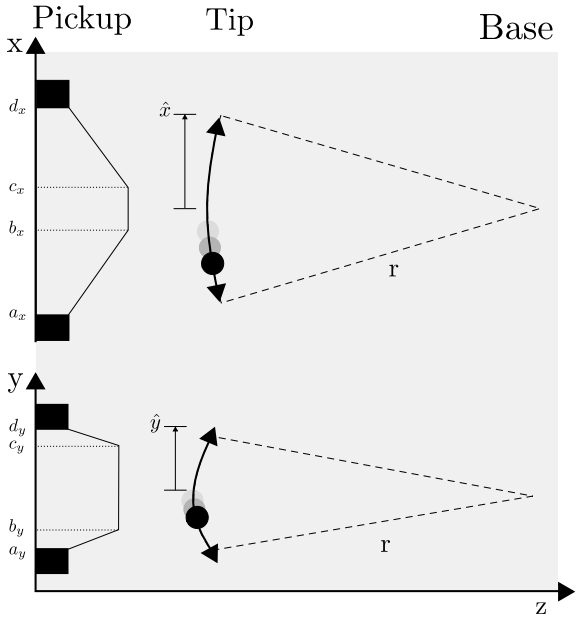

Figure 6: Simplified geometry of the pickup system and the vibrating tine in the x- and y-plane orthogonal to the magnetic pick-up.

Defining an imaginary magnetic point charge which induces a change in the magnetic flux in the direction of z

$$\mathbf{B}_z = B_0 \frac{\Delta z}{|r_{21}|^3} \tag{6}$$

The magnetic field for position $(x^{'}, z^{'})$ in front of the of steel tip can thus be written as a three-part integral

$$\begin{aligned} \mathbf{B}_z(x^{'}, z^{'}) \quad &= \quad |\mathbf{B}_{tine}| \\ &\cdot \quad \Big[\int_a^b \frac{\sigma(z^{'} - z(x))x}{[(x' - x)^2 + (z' - z(x))^2]^{3/2}} dx \\ &+ \quad \int_b^c \frac{\sigma(z^{'} - z_k)x}{[(x' - x)^2 + (z' - z_k)^2]^{3/2}} dx \\ &+ \quad \int_c^d \frac{\sigma(z^{'} - z(x))x}{[(x' - x)^2 + (z' - z(x))^2]^{3/2}} dx \Big] \end{aligned} \tag{7}$$

with σ the constant magnetic charge density the magnetic field distribution for position $(y^{'}, z^{'})$ can be computed accordingly. Integrating this formula for all points on a trajectory given by the position of the Rhodes' tine tip

$$\begin{aligned} z^{'} \quad &= \quad \mathrm{r} - \sqrt{\mathrm{r}^2 - (x')^2} \\ x^{'} \quad &= \quad \hat{\mathrm{x}} \cdot sin(2\pi f_{tine} t) \end{aligned} \tag{8}$$

[1] This assumption proposes an equivalence between the effective causes of electric fields and magnetic fields and can be used as a mathematical modeling tool, see: [31, pp. 174 ff].

with f_{tine} the fundamental frequency of the tine, leads to a magnetic potential function characterising the magnitude of relative magnetic field change.

An idealised form of the magnetic field in front in one plane of the Rhodes pickup is depicted in Figure 7**a** and 7**b**, it is comparable to the measurements results published in [16].

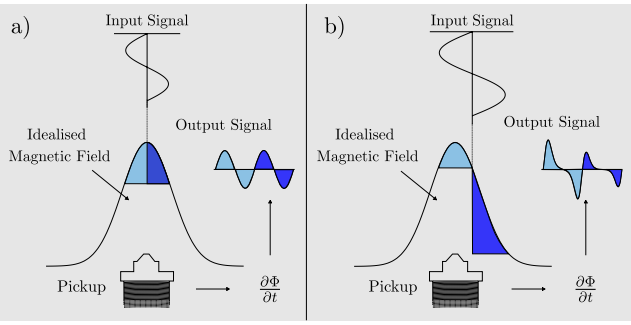

Figure 7: An idealised schematic depiction of the pickup system of the Rhodes E-piano. The sinusoidal motion of the vibrating tine induces a c **a**) A low amplitude input of a sinusoidal vibration of the magnetic flux weighted by the magnet fields distribution. By differentiating the magnetic flux in respect to time, the alternating voltage present at the output is calculated. **b**)A similar model setup as before consisting of a slightly displaced mid-point for the input motion resulting in a different weighting function of the magnetic field. The output shows a different form than before. This condition is close to a realistic playing condition found in Rhodes E-pianos.

5.5. Wurlitzer reed model

The reed of the Wurlitzer is modeled using a similar PDE as for the Rhodes' tine using only one direction of motion u, the coupling term between the two polarisations is ommited. The use of a beam model instead of a plate model is justifiable here because typical effects found in plates were not measured using the high-speed camera setup and thus are either not present or small compared to the transversal deflection of the fundamental mode. In addition to that, the measurements show that the influence of higher modes are comparably small or non-existent even under extreme playing conditions, thus the primary mode of vibration can be approximated by the reeds first natural frequency which coincides with a cantilever beam of similar dimensions.

$$\rho u_{tt} + [\mathrm{EI}u_{xx}]_{xx} - \kappa u_{2x2t} - f(x,t) = 0$$

with the same variables as introduced before. Again Equation 9 does not explicitly depend on the shear angle α (see [28]) thus it is not regarded here any further. Again omitting the shear angle, the boundary conditions for the fixed/free beam are

$$\begin{aligned} u|_0 &= 0 \\ \mathrm{k}^{'}\mathrm{GA}u_x|_L &= 0\,. \end{aligned} \tag{9}$$

5.6. Wurlitzer pickup model

The influence of the Wurlitzer's pick-up system can be characterised as a change in capacitance of a time varying capacitor induces an alternating voltage which is amplified as the instruments sound. Using a basic definition of time-varying capacitance that induces a current i we get

$$i(t) = \mathrm{C(t)}\frac{\partial \mathrm{u}(t)}{\partial t} + \mathrm{u(t)}\frac{\partial \mathrm{C}(t)}{\partial t} \tag{10}$$

with u the voltage and C the capacitance both depending on time t. For the derivation of the influence function of the capacitor we take two simplifying assumptions.

1. The time dependent charging / discharging curve of the capacitor is linear in the considered range.
2. The supply voltage stays constant during a capacity change cycle of the capacitor.

Using both definitions, we can write the time-dependent current resulting from a changing capacitance as

$$i(t) = \mathrm{u}_0\frac{\partial \mathrm{C}(t)}{\partial t} \tag{11}$$

This alternating current induces an alternating voltage over a resistor that drives an amplification circuit.

To calculate the capacitance curve due to the deflection of the Wurlitzer's reed, a number of i planes through the geometry are taken and the electric field strength is computed for each resulting slice simplifying the 3-dimensional problem to a 2-dimensional. The capacitance for each slice can be computed from the electric field by

$$C_i = \frac{Q_i}{U_i} \tag{12}$$

with $Q_i = \epsilon_t \oint_A \vec{\mathbf{E}} \cdot \mathrm{d}\mathbf{A}$ the charge defined as the integral of the electric field over the surfaces of the geometries using Gauss's theorem and ϵ_t an electric field constant for the material and free field properties. Three exemplary positions for the computation of the capacitance are depicted in Figure 8.

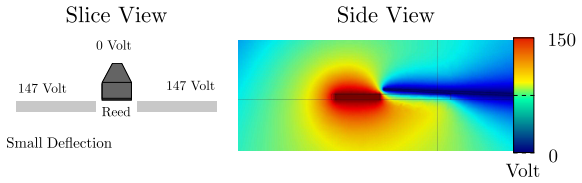

Figure 8: Distribution of the electric field for one examplary reed deflections. On the left hand side one slice of geometry on the right hand side the results from an FEM model.

6. HARDWARE MODEL

6.1. Overview

The finite difference implementations of the physical models described in section 5 are implemented on an FPGA development board consisting of a XILINX Virtex-7 690T. This section gives a short overview on the methodology and the implementation of the real-time hardware models. A more detailed account is published in [21] or [34]

6.2. FPGA hardware overview

The real-time implementations presented in this work, make use of the parallel structure of an FPGA using a concurrent iterative approach for basic computations of all numerical schemes.

The parallel processing capabilities of FPGAs are mainly due to their inherently parallel hardware structure. The core parts of FPGAs consist of freely programmable, interconnected logic cells that can perform several Boolean operations (AND, OR, XOR...) depending on input and configurations signals. Most modern FPGAs employ Look-Up-Tables (LUTs) which act as addressable function generators having a number of logic inputs and logic outputs performing a specified Boolean operation [**?**]. Interconnecting these basic logic blocks, more complex logic functions can be realized ranging from basic arithmetic operations to specialised processing units.

6.3. FD Models on FPGA Hardware

To take benefit from the inherently parallel structure of FPGA hardware central parts of the FD models introduced in this work are processed in parallel. The numerical schemes developed in (5) can be split into sequential and parallel parts. The sequential computation is necessary for the interdependent computations of the velocities and the deflection of one discretised FD node on a geometry. When processed with synchronous timing, all FD nodes can be computed concurrently leading to an numerical scheme which can be efficiently computed on FPGA hardware.

The real-time implementations of the proposed FD models make use of a structured design approach consisting of a layer model developed to combine functional parts of FD models and assort them according to their respective functionality. All partitions of the FPGA implementations are categorised into five different sub-layers, each encapsulating specific functionality, specific data types and a specific communication protocol [21]. This layer model enables the reuse of structurally similar parts of different models minimizing implementation efforts for new FD designs.

Both instrument models are implemented by transferring the FD models developed before to a hardware level. This can be realised by rewriting the finite difference schemes using a hardware operator notation explained below. All basic numerical computations are implemented on the Algorithmic Layer, the structure of the modeled geometry is initialised and parametrised on the Model Routing Layer. The functionality of the other layers include signal routing, timing and synchronisation of the computation and simulated signals.

A structural flow diagram given in Figure 9 shows that both models share similarities regarding their processing steps.

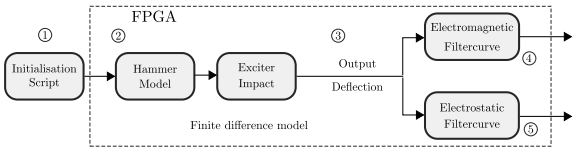

Figure 9: Schematic depiction of the processing chain of the model. ① The respective model is initialised regarding its physical properties and boundary condition. ② Computation of the finite difference models on FPGA hardware. ③ Output of the respective exciter model. ④ Rhodes model output. ⑤ Wurlitzer model output.

6.4. Discrete FD Operators

As extension to the well-established FD operator notation (see [32]; [30] or [29] a discrete operator formalism is used in this work. The operator notation allows to transfer several mathematical operation into a simpler notation. In the following, this concept is extended to an even lower abstraction level by resolving the underlying mathematical operations to the specific operations depending on the data type and underlying hardware structure. Assuming a signed two's complement data type, a centered finite difference operator can be expressed with following statement

$$\hat{\delta}_x = T_\Delta \cdot [\hat{\epsilon}_{\Delta x+}, -\hat{\epsilon}_{\Delta x-}] \tag{13}$$

with $\hat{\epsilon}_{\Delta x+/\Delta x-}$ = a read operation from a register a finite difference cell right (+) or left (-) of the actual cell and T_Δ a multiplicand which depends on the stride of the discrete grid in the spatial domain. A second order centered FD operator in vector notation can be written as

$$\hat{\delta}_{xx} = T_\Delta \cdot [(\hat{\epsilon}_{\Delta x-}), (<1), (\hat{\epsilon}_{\Delta x+})] \tag{14}$$

with $T_\Delta = \frac{1}{\Delta x}$ and (<1) indicating a shift operation. This shift operation can be used to replace a multiplication by 2 in fixed-point arithmetic. A higher order digital FD-operator used for the fourth order differential equation of the beam can be constructed by a convolution of two second order digital FD operators

$$\hat{\delta}_{4x} = \hat{\delta}_{xx} * \hat{\delta}_{xx}. \tag{15}$$

This can be extended to higher spatial order difference operators leading to a specific numbers of digital operations for the respective operator given in Table 1. These basic operators can be em-

??

Table 1: Digital operations for FD operators used in this work

Operator	Reg. Op.	Shift Op.	Mult.	Add./Sub.
$\hat{\delta}_x$	2	0	1	2
$\hat{\delta}_{xx}$	3	1	1	2
$\hat{\delta}_{4x}$	5	4	1	5
$\hat{\delta}_{2x2y}$	5	1	1	4

ployed for temporal as well as spatial discretisation and can be extended by including variable as well as static multiplicands into the formulation. For reasons of brevity, all material parameters of the following models are included in the operator notation as multiplicands and are preprocessed during model initialisation. Hence, a second order operator still needs one multiplication including material and geometry dependant weighting.

6.5. Finite difference hardware models

The exciter models of the Rhodes and the Wurlitzer pianos are discretised applying standard finite difference approximations using a symplectic Euler scheme for iteration in time. The discretisation method and the scheme are published in more detail in [21] and [20]. Applying the presented hardware FD approximations from Table 1 and splitting the PDE by introducing $v_1 = u\_t$, the transverse part of Equation 2 can be written as

$$\begin{aligned} \hat{\delta}_t v &= [-\hat{\delta}_{xx} + \hat{\delta}_{tt}]\hat{\delta}^M_{xx}\mathbf{u} + K(\mathbf{u}, \mathbf{v}, t) + F([\mathbf{x}], t) \\ \hat{\delta}_t u &= v \end{aligned} \tag{16}$$

7. SIMULATION RESULTS

7.1. Interaction with the model

Both real-time models can be controlled and parametrized using a script file. Besides controlling physical properties of the tone generators, initial values of the hammer can be set. A keyboard interface implementing the OSC protocol to interact with the models is a work in progress.

7.2. Simulation results Rhodes model

The following examples show simulation results of the real-time model parametrized with different initial conditions.

Increasing hammer velocities

Figure 10 shows five simulated Rhodes notes with varying start velocities the hammer model. This simulation shows that increasing the impact velocity of the hammer, increases the complexity of the Rhodes' due to the effects shown in Figure 7.

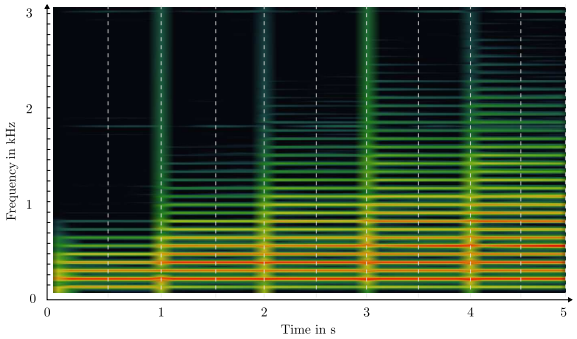

Figure 10: Spectrogram of a Rhodes model impacted with increasing hammer velocity.

2 dimensional polarisation

One of the effects that can be modeled using the extended formulation of the Rhodes' tine presented in this paper is the possibility to simulate two-dimensional vibrations of the impacted Rhodes tine

Figure 11 depicts the simulated deflection of both horizontal polarizations of the tine. When compared to the measurements given in Figure 4 it is obvious that the simulated coupling mechanism is capable of representing the measured behaviour of the tine.

Tuning of a Wurlitzer reed

In this simulation, the amount of solder on the Wurlitzers reed is changed by altering the mass distribution at the tip of the reed (see Figure 2 for a schematic depiction of the reed). As shown in Figure 12, changing the amount of solder leads to a detuning of the fundamental vibration frequency.

8. CONCLUSIONS

In this paper a real-time implementation of main sound producing parts of the Rhodes and Wurlitzer electronic pianos was presented.

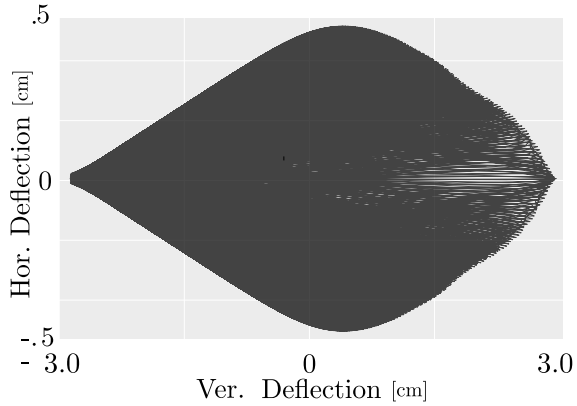

Figure 11: Horizontal vs. vertical deflection of an hammer impacted Rhodes tine.

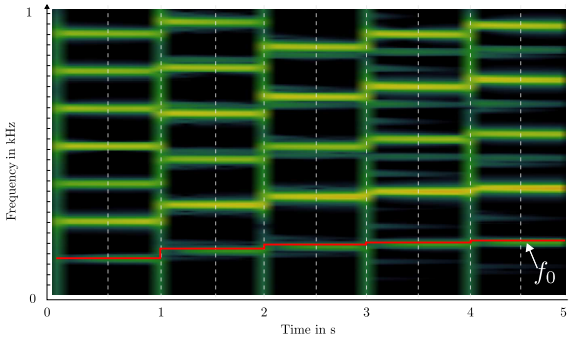

Figure 12: Spectrogram of five synthesized Wurlitzer notes. Every second, the mass on the tip is increased, thereby simulating the tuning procedure as described in section 3.

Both instruments are based on physical models and are computed on a an FPGA board which is connected to a standard personal computer and can be played and parametrized in real-time.

The presented models are able to capture salient features of the instruments and make it possible to interact with physical properties and parameters. Regarding the expressive range, both modeled instruments capture essential parts of the sound characteristics and can help in understanding specific features of both instruments in more detail.

Nonetheless, there are several parts in the model formulation which work with simplifications especially the physical properties of the respective pick-up systems. A further step to enhance this work would be an inclusion of a geometrically accurate model of the Rhodes electromagnetic pick-up and the Wurlitzer's electrostatic pick-up system.

9. ACKNOWLEDGMENTS

I would like to thank the anonymous reviewers. This work was partially funded by the *Deutsche Forschungs Gemeinschaft* DFG hence it gives me great pleasure to acknowlede their support.

10. REFERENCES

[1] A. Kovetz, "The Principles of Electromagnetic Theory", Cambridge University Press, 1990.

[2] Jianming Jin, "The Finite Element Method in Electromagnetics", 2nd ed., Wiley-IEEE Press, May 2002.

[3] D.K. Cheng, "Field and Wave Electromagnetics, 2nd ed.", Addison-Wesley, 1991.

[4] Anthony C. Ippolito, "Electronic piano feedback reduction", US 3435122 A, 1965

[5] Harold B. Rhodes, "Electrical musical instrument in the nature of a piano", U.S. Patent 2,972,922, 1961.

[6] Harold B. Rhodes, "Piano Action", U.S. Patent 4,338,848, 1982.

[7] Harold B. Rhodes and James B. Murphy, "Multiple Voice Electric Piano And Method", U.S. Patent 4,342,246, 1982.

[8] Harold B. Rhodes and Steven J. Woodyard,"Tuning Fork Mounting Assembly In Electromechnanical Pianos", U.S. Patent 4,373,418, 1983.

[9] Greg Shear and Matthew Wright,"The electromagnetically sustained Rhodes piano", NIME Proceedings, Oslo, 2011.

[10] Torsten Wendland, "Klang und Akustik des Fender Rhodes E-Pianos", Technische Universität Berlin, Berlin, 2009.

[11] Rhodes Keyboard Instruments, "Service Manual", CBS Musical Instruments a Division of CBS Inc., Fullerton CA, 1979.

[12] Benjamin F. Miessner, "Method and apparatus for the production of music", US Patent 1,929,027, 1931.

[13] C.W. Andersen, "Electronic Piano", US 2974555, 1955.

[14] Federico Avanzini and Davide Rocchesso. Physical modeling of impacts: theory and experiments on contact time and spectral centroid. In *Proceedings of the Conference on Sound and Music Computing*, pages 287–293, 2004.

[15] Tatsuya Furukawa, Hideaki Tanaka, Hideaki Itoh, Hisao Fukumoto, and Masashi Ohchi. Dynamic electromagnetic Analysis of Guitar Pickup aided by COMSOL Multiphysics. In *Proceedings of the COMSOL Conference Tokyo 2012*, Tokyo, 2012. COMSOL.

[16] Nicholas G. Horton and Thomas R. Moore. Modeling the magnetic pickup of an electric guitar. *American Journal of Physics*, 77(2):144, 2009.

[17] Malte Muenster and Florian Pfeifle. Non-Linear Behaviour in Sound Production of the Rhodes Piano. In *Proceedings of the International Symposium of Musical Acoustics (ISMA) 2014*, pages 247–252, Le Mans, France., 2014.

[18] Florian Pfeifle and Malte Muenster Tone Production of the Wurlitzer and Rhodes E-Pianos In Albrecht Schneider, editor, *Studies in Musical Acoustics and Psychoacoustics* volume 5 of *Current Research in Systematic Musicology*, pages 75–107. Springer International Publishing, 2017.

[19] Malte Muenster, Florian Pfeifle, Till Weinrich, and Martin Keil. Nonlinearities and self-organization in the sound production of the Rhodes piano. *The Journal of the Acoustical Society of America*, 136(4):2164–2164, 2014.

[20] Florian Pfeifle. Multisymplectic Pseudo-Spectral Finite Difference Methods for Physical Models of Musical Instruments. In Rolf Bader, editor, *Sound - Perception - Performance*, volume 1 of *Current Research in Systematic Musicology*, pages 351–365. Springer International Publishing, 2013.

[21] Florian Pfeifle and Rolf Bader. Real-Time Finite-Difference Method Physical Modeling of Musical Instruments Using Field-Programmable Gate Array Hardware. *J. Audio Eng. Soc*, 63(12):1001–1016, 2016.

[22] Anatoli Stulov. Hysteretic model of the grand piano hammer felt. *The Journal of the Acoustical Society of America*, 97(4):2577–2585, 1995.

[23] Roald K. Wangsness. *Electromagnetic fields*. Wiley, New York, 2nd ed edition, 1986.

[24] Steve Espinola. Wurlitzer Electric Piano models: a list. | Paleophone. Blog entry Available at: `http://paleophone.net/?page_id=923`. (Accessed: 23rd May 2016)

[25] Wurlitzer Company, The Electric Pianos Series 200 and 200A Service Manual Available at: `http://manuals.fdiskc.com/flat/Wurlitzer%20Series%20200%20Service%20Manual.pdf` (Accessed: 17.02.2016)

[26] R. W. Traill-Nash and A. R. Collar. The effects of shear flexibility and rotatory inertia on the bending vibrations of beams. *The Quarterly Journal of Mechanics and Applied Mathematics*, 6(2):186–222, 1953.

[27] Antoine Falaize and Thomas HÃ©lie. Passive simulation of the nonlinear port-Hamiltonian modeling of a Rhodes Piano. *Journal of Sound and Vibration*, 390:289–309, March 2017.

[28] Seon M. Han, Haym Benaroya, and Timothy Wei. Dynamics of transversely vibrating beams using four engineering theories. *Journal of Sound and Vibration*, 225(5):935–988, September 1999.

[29] Stefan D. Bilbao. *Numerical sound synthesis: finite difference schemes and simulation in musical acoustics*. Wiley, Chichester, 2009.

[30] Charles Jordan. *Calculus of finite differences*. Chelsea Publ. Co, New York, 1 edition, 1950.

[31] John D. Jackson *Classical Electrodynamics* John Wiley & sons, Inc., 3rd edition, 1998

[32] John C. Strikwerda. *Finite Difference Schemes and Partial Differential Equations, Second Edition*. Society for Industrial and Applied Mathematics, Philadelphia, USA, 2nd ed edition, 2004.

[33] K. H. Hunt and F. R. E. Crossley. Coefficient of restitution interpreted as damping in vibroimpact. *Journal of applied mechanics*, 42(2):440–445, 1975.

[34] F. Pfeifle *Physical Model Real-time Auralisation of Musical Instruments: Analysis and Synthesis* Ph.D. Dissertation. University of Hamburg. 2014.